

# Stabilization of Buoyancy-Driven Unstable Vortex Flow in Mixed Convection of Air in a Rectangular Duct by Tapering Its Top Plate

W. S. Tseng  
W. L. Lin  
C. P. Yin  
C. L. Lin  
T. F. Lin

Department of Mechanical Engineering,  
National Chiao Tung University,  
Hsinchu, Taiwan, R.O.C.

*Stabilization of the buoyancy-driven unstable mixed convective vortex air flow in a bottom heated rectangular duct by tapering its top plate is investigated experimentally. Specifically, the duct is tapered so that its aspect ratio at the duct inlet is 4 and gradually raised to 12 at the exit of the duct. In the study the secondary flow in the duct is visualized and the steady and transient thermal characteristics of the flow are examined by measuring the spanwise distributions of the time-average temperature. The effects of the Reynolds and Grashof numbers on the vortex flow structure are studied in detail. Moreover, the spanwise-averaged Nusselt numbers for the horizontal rectangular and tapering ducts are also measured and compared. Furthermore, the time records of the air temperature are obtained to further detect the temporal stability of the flow. Over the ranges of the  $Re$  and  $Gr$  investigated for  $5 \leq Re \leq 102$  and  $1.0 \times 10^4 \leq Gr \leq 1.7 \times 10^5$ , the vortex flow induced in the rectangular duct exhibits temporal transition from a steady laminar to time periodic and then to chaotic state at increasing buoyancy-to-inertia ratio. Substantial change in the spatial structure of the vortex flow is also noted to accompany this temporal transition. The results for the tapering duct indicate that more vortex rolls can be induced due to the increase in the aspect ratio of the duct with the axial distance. But the vortex rolls are weaker and are completely stabilized by the tapering of the top plate.*

[S0022-1481(00)70301-X]

*Keywords:* Heat Transfer, Mixed Convection, Vortex

## 1 Introduction

At high buoyancy-to-inertia ratio frequently encountered in various heat transfer equipment, the buoyancy-driven secondary vortex flow in a forced laminar flow through a bottom heated rectangular duct is rather unstable. Heat transfer augmentation associated with the buoyancy-driven vortex flow is desirable and welcome in many technological applications in which the efficient energy transport is of major concern. However, in the chemical vapor deposition (CVD) processes used to grow thin crystal films on semiconductor substrates, the presence of the vortex flow at a high buoyancy and a low inertia for the Reynolds number ranging from 1 to 100 will result in a nonuniform chemical vapor deposition, producing a thin crystal film of nonuniform thickness. Moreover, the unsteady vortex flow will provoke a time-dependent deposition rate. These unsteady vortex flows are not welcome and should be avoided in the CVD processes. A simple mean often used to suppress and stabilize the vortex flow is to accelerate the main flow so that the buoyancy-to-inertia ratio decreases in the flow direction. This experimental study intends to explore the change in the vortex flow structure of air caused by the flow acceleration when the top plate of a bottom-heated horizontal rectangular duct is slightly tapered.

In a horizontal parallel plane channel with the bottom plate at a higher uniform temperature than the top one by  $\Delta T$ , the critical Rayleigh number for the onset of the vortex flow was found to be around 1708, as predicted from experimental measurements and linear stability theory ([1,2]). Ostrach and Kamotani [3] and Kamotani and Ostrach [4] experimentally noted that the longitudinal vortex rolls appear when the temperature difference becomes

larger than a critical value corresponding to  $Ra = 1708$ . Above the critical point, the heat transfer rate is increased by the thermal instability and the temperature field is strongly influenced by the motion of the vortex rolls. When  $Ra > 8000$ , the vortex rolls become irregular. Hwang and Liu [5] visualized the onset of secondary flow and showed that the wave number of vortex rolls remains constant along the flow direction. Experiments conducted by Incropera et al. [6] and Maughan and Incropera [7] disclosed four flow regimes along the bottom plate-laminar forced convection, laminar mixed convection, transitional mixed convection, and turbulent free convection. The transition to turbulent flow was attributed to the breakdown of the vortices due to the hydrodynamic instability. Besides, a correlation for the onset points was proposed. Criteria for the onset of vortex instability and the start of the transition from two-dimensional laminar flow to three-dimensional vortex flow in mixed convection air flow over an isothermally heated horizontal flat plate were established by Moharreri et al. [8]. The vortex flow regime started with a stable laminar flow region where vortices develop and grow gradually and ended with an unstable flow region where the vortices mix together and collapse to form a two-dimensional turbulent flow regime.

In the mixed convection of the nitrogen gas between two horizontal, differentially heated parallel plates, Chiu and Rosenberger [9,10] showed that the critical  $Ra$  for the appearance of the transverse convection rolls increased with  $Re$ . They also found that at a high  $Ra$ , the longitudinal rolls were unsteady and snaking. Besides, they showed the regime of  $Ra$  and  $Re$  leading to a steady or unsteady flow. Nyce et al. [11] showed the variations of velocity field in both the axial and transverse directions which were consistent with the presence of both longitudinal roll and transverse wave instabilities. The transverse rolls were noted at a very low Reynolds number by Ouazzani et al. [12,13]. They also refined the regime map to include the transverse rolls. The recent flow visualization from Yu et al. [14] showed that at a fixed  $Ra$  but in

Contributed by the Heat Transfer Division for publication in the JOURNAL OF HEAT TRANSFER. Manuscript received by the Heat Transfer Division, Feb. 7, 1999; revision received, July 27, 1999. Associate Technical Editor: F. Cheung.

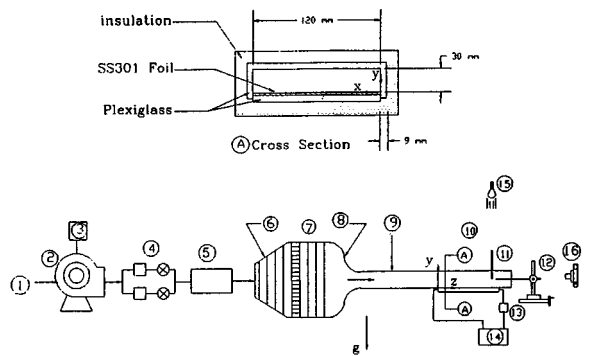
reducing  $Re$  the vortex flow transforms from the structure prevailed by the longitudinal rolls to transverse waves in sequence of stable longitudinal rolls, unstable longitudinal rolls, mixture of the longitudinal rolls and transverse waves, and transverse waves. Photographic results from Cheng and Shi [15] revealed the convective instability and chaotic phenomena caused by the buoyancy forces. Koizumi and Hosokawa [16] presented the sidewall temperature profile in a horizontal rectangular duct heated from below which simulated a horizontal thermal CVD reactor. They found that although the flow was unsteady but the time-averaged local mass transfer rate on the bottom wall can be almost uniform.

Recently, in a series of studies ([17–20]) we unraveled the complex flow characteristics in an air flow through a bottom-heated horizontal rectangular duct of aspect ratio  $AR=2$  & 4. The formation, merging, and splitting of the longitudinal vortex rolls were numerically and experimentally predicted for the laminar steady, laminar time periodic, transitional quasi-periodic, and irregular chaotic flow at increasing buoyancy-to-inertia ratio.

The above literature review clearly reveals that there has been a substantial amount of research carried out in the past on various aspects of the vortex flow and heat transfer in mixed convection of gas in a horizontal rectangular duct. However, very little is known on the processes of how the vortex flow is suppressed by the flow acceleration resulting from reducing the cross-sectional area of the duct. An experimental investigation combining flow visualization and temperature measurements will be conducted in the present study to unravel the effects of tapering the top plate of rectangular duct on the detailed changes in the vortex flow structure in a mixed convective air flow through a bottom heated trapezoid duct. Attention will be focused on the flow stabilization and weakening of the vortex flow by the acceleration of the primary flow for various Reynolds and Grashof numbers.

## 2 Experimental Apparatus and Procedures

**2.1 Experimental Apparatus.** Figure 1 shows a schematic arrangement of the mixed convective experimental apparatus established for the present study. The apparatus consists of three parts: wind tunnel, test section, and measuring probes along with a data acquisition unit. Two different test sections have been designed, one for the rectangular duct without tapering the top plate and another for the trapezoid duct with the top plate tapered downwards from the duct inlet to exit. The test section for the rectangular duct is constructed of 9-mm-thick plexiglass top and side walls to facilitate flow visualization. The rectangular cross section is 30 mm in height and 120 mm in width and the duct has a total length of 800 mm, providing an aspect ratio of  $AR=4$  for the duct. The tapering duct is also 800 mm long and is made of



1. air flow ; 2. blower ; 3. frequency regulator ; 4. flowmeters and valves ; 5. smoke container ; 6. diffuser with screens ; 7. straightener with honeycomb and screens ; 8. nozzle ; 9. developing channel ; 10. test section ; 11. probes ; 12. three-way traversing device ; 13. ammeter ; 14. D.C. power supply ; 15. lamp ; 16. camera.

Fig. 1 Schematic diagram of the experimental apparatus

10-mm-thick plexiglass top and 9-mm-thick plexiglass side walls. The top plate is inclined downwards so that the aspect ratio of the duct cross section increases from 4 at the inlet to 12 at the exit with the duct height reduced from 30 mm at the inlet to 10 mm at the exit. The inclined angle of the top plate is rather small at 1.432 deg when measured from the horizontal. The details of the mixed convective loop were already described in Lin and Lin [19]. Besides, the experimental procedures and method to analyze the temperature fluctuation were also given in that study.

**2.2 Data Reduction for Heat Transfer Coefficient.** The spanwise-averaged Nusselt number defined as

$$Nu_d = \frac{hd_{in}}{k} = \frac{q''_{conv}d_{in}}{(\bar{T}_w - T_{in})k} \quad (1)$$

is obtained from measuring the spanwise-averaged bottom wall temperature  $\bar{T}_w$  and local convective heat flux  $q''_{conv}$ . Note that the heat transfer coefficient  $h$  is based on the temperature difference  $(\bar{T}_w - T_{in})$  instead of  $(\bar{T}_w - T_b)$  since the heated section is not long ( $L/d_{in}=26.7$ ) and the convective heat transfer in it mainly takes place in the entrance region. The surface energy balance relating the total energy dissipated in the heater plate due to the electric resistance heating per unit surface area  $q''_{tot}$  to the heat fluxes associated with the convection from the surface to the flow  $q''_{conv}$ , net radiation heat loss from the surface  $q''_{rad}$  and conduction loss through the insulation  $q''_{insul}$  is

$$q''_{tot} = q''_{conv} + q''_{rad} + q''_{insul} \quad (2)$$

The convective heat flux is therefore determined by measuring the total dissipated heat flux and applying appropriate correlations for the nonconvective components. An implication of the expression in Eq. (2) is that although uniform heat generation  $q''_{tot}$  is achieved in the heated plate, variations in the radiation and conduction losses with the location induce nonuniformities in the convective heat flux. The axial variations in  $q''_{conv}$  were estimated to be less than 20 percent of the average  $q''_{conv}$ . The radiation and conduction losses were estimated to range from 32 percent to 36 percent and 13 percent to 17 percent, respectively.

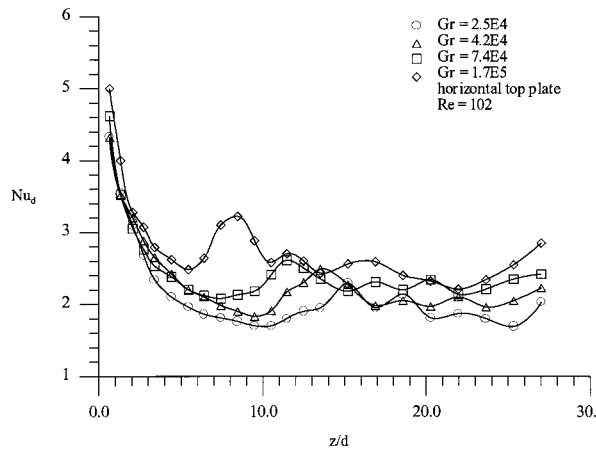
Uncertainties in the Nusselt, Reynolds, and Grashof numbers were estimated according to the standard procedures proposed by Kline and McClintock [21]. This analysis indicated that through the combination of many measurements together with the uncertainties in the conductive and radiative losses, the uncertainties in  $Re$ ,  $Gr$ , and  $Nu_d$  are 2 percent, 11 percent, and 4 percent, respectively.

## 3 Discussion of Experimental Results

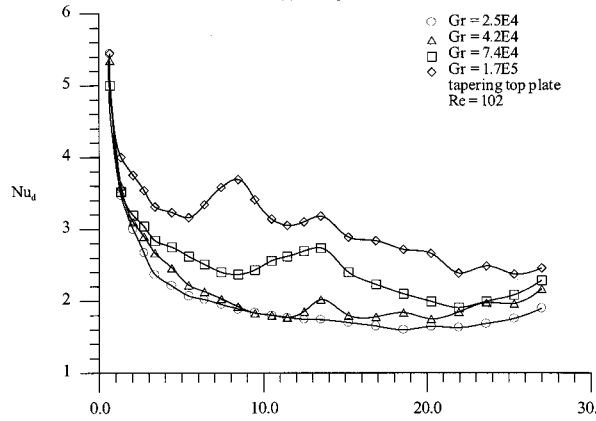
In what follows, only a small sample of the results obtained are presented to illustrate the effects of the top plate tapering on the flow stabilization by examining the resulting vortex flow structures and time history of the air temperature. In addition, the spanwise average Nusselt number affected by the plate tapering is also inspected. More detailed results are available from the thesis of Tseng [22].

**3.1 Spanwise Average Heat Transfer Coefficient.** The axial distributions of the steady spanwise average Nusselt number was obtained first for the limiting cases of forced convection with the Grashof number  $Gr (= g\beta q''_{conv}d_{in}^4/k\nu^2)$  below 2000 for the rectangular and tapering ducts. The data for the rectangular duct were very close to that calculated for the forced convection in that duct from the previous numerical computation ([18]). This was verified in our previous studies ([19,20]). In the exit region the Nusselt number for the tapering duct is slightly above that for the rectangular duct due to the acceleration of the main flow.

Effects of the Grashof number on the time-averaged axial variations of the spanwise average Nusselt number in the two different



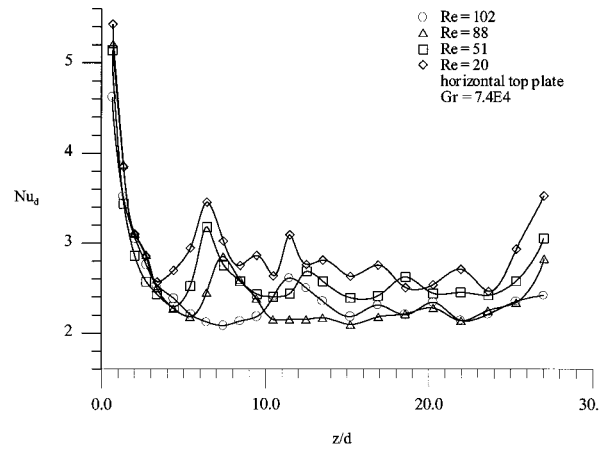
(a)rectangular duct



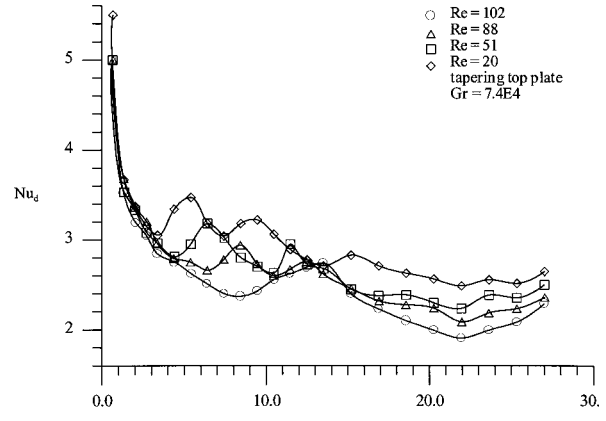
(b)tapering duct

**Fig. 2** Effects of Grashof number on the spanwise-averaged Nusselt number distribution for  $Re=102$  for (a) rectangular duct and (b) tapering duct

ducts are shown in Fig. 2 for  $Re=102$ . The results in Fig. 2(a) for the horizontal top plate indicate that at a given  $Gr$  near the duct entry the Nusselt number decreases monotonically in the flow direction. At a certain axial location  $Nu_d$  reaches a minimum and rises gradually. This location corresponds to the onset of the buoyancy-induced vortex flow. More specifically, the onset point is defined as the axial station where the spanwise average Nusselt number enhanced by the vortex flow exceeds that for the forced convection by three percent. At a higher Grashof number this onset location appears at a shorter distance from the duct inlet. The monotonic decay in the Nusselt number in the upstream is associated with the dominated laminar forced convection there. Beyond the onset point plumes of warm fluid rise from the heated surface resulting in a developing secondary flow and the plate temperature is reduced by the cool air descending from the duct core. Thus, the flow circulation provides an effective mechanism for heat transfer enhancement. As the secondary flow strengthens, the Nusselt number rises well above the forced convection limit. Further downstream the core flow has been warmed up and  $Nu_d$  reverses its trend to decrease in the flow direction. Thus, we have oscillatory  $Nu_d$  distributions in the axial direction for a high  $Gr$ . The results for the tapering duct (Fig. 2(b)) resemble those for the rectangular duct (Fig. 2(a)) except that in the tapering duct the onset of the vortex flow moves a little downstream as compared with that for the horizontal duct for the same  $Re$  and  $Gr$ . Note that the duct height at the duct inlet is used in defining  $Gr$  for the tapering duct. It is further noted that the axial rise in  $Nu_d$  due to the vortex flow are slightly smaller for the tapering duct, implying the induced secondary flow being weaker. Also note that  $Nu_d$  is



(a)rectangular duct



(b)tapering duct

**Fig. 3** Effects of Reynolds number on the spanwise-averaged Nusselt number distribution for  $Gr=7.4 \times 10^4$  for (a) rectangular duct and (b) tapering duct

lower for the tapering duct in the downstream region of the duct. These results indicate that the Nusselt number increases with the Grashof number except in the region near the exit of the tapering duct. Near the exit region, the flow accelerates so rapidly that the transport process is dominated by forced convection. Therefore, the Grashof number only exhibits a mild effect on the heat transfer near the duct exit.

The data in Fig. 3 for illustrating the effects of the Reynolds number on the  $Nu_d$  distributions for both ducts indicate that the onset of secondary flow moves downstream at increasing Reynolds number for  $Gr$  fixed at  $7.4 \times 10^4$ . This trend is in compliance with the fact that the velocity boundary layer gets thinner at a higher  $Re$  and thereby increases its resistance to thermal instability, and hence impedes secondary flow development. Oscillatory  $Nu_d$  variations with the axial distance are also noted for these curves. More intense oscillations result for a higher buoyancy-to-inertia ratio. Moreover, at the same  $Re$  and  $Gr$  the onset point moves downstream in the tapering duct as compared with that for the corresponding case in the rectangular duct. Besides,  $Nu_d$  is also lower in the tapering duct.

It is of interest to note that the onset points for various cases covered here for both ducts can be correlated as

$$Gr_z = 3637 Re_z^{1.66} \quad (3)$$

where  $Gr_z$  and  $Re_z$  are the local Grashof and Reynolds numbers,  $Gr_z = g \beta q''_{conv} z^4 / k v^2$  and  $Re_z = \bar{w} z / \nu$ . Here  $\bar{w}$  is the local mean velocity of the air in the ducts, which increases linearly with the axial distance for the tapering duct. But for the rectangular duct  $\bar{w}$  is constant.

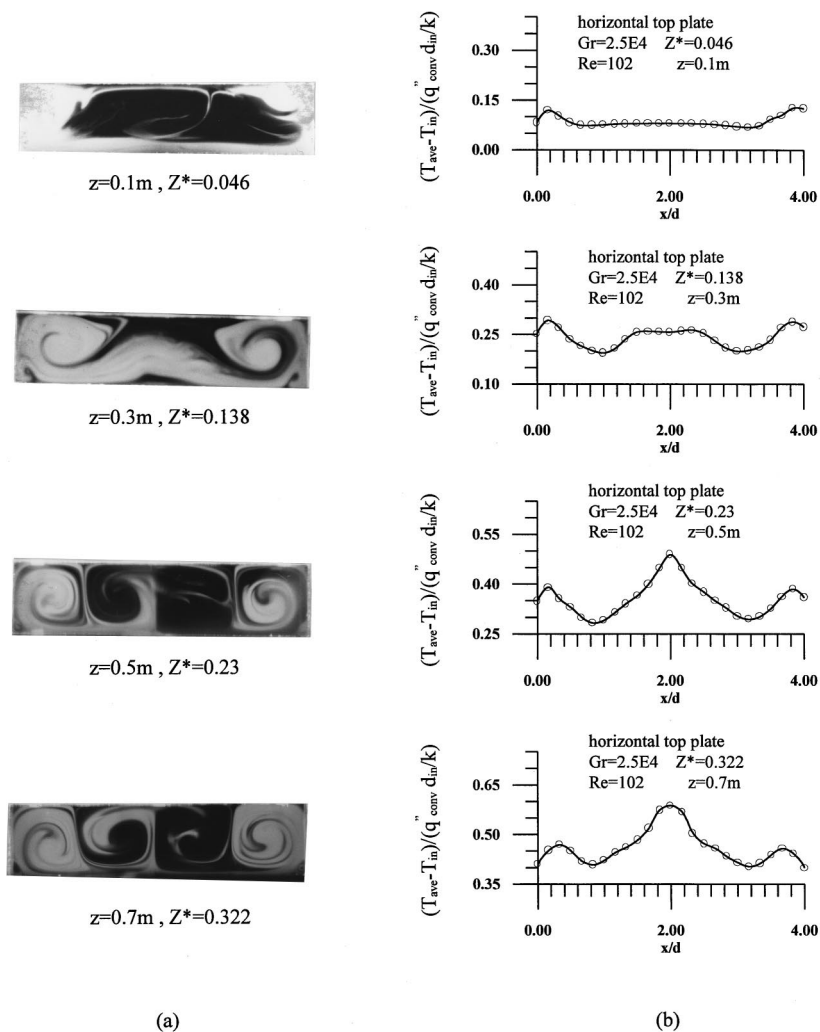


Fig. 4 (a) Instantaneous flow photos and (b) time-averaged spanwise temperature distributions at  $y=1.5$  cm at selected cross sections in rectangular duct for  $Re=102$  and  $Gr=2.5 \times 10^4$

**3.2 Vortex Flow Structure and Spanwise Temperature Distributions.** Flow visualization was conducted to detect the resulting buoyancy-induced vortex flow patterns at steady or statistical state for both rectangular and tapering ducts for various Reynolds and Grashof numbers. They were carried out by using a 1.5–3-mm plane light beam shone through the flow field containing small incense smoke particles as light scattering centers.

Side views of the instantaneous flow photos taken at the central vertical plane at  $x=6$  cm for various Reynolds and Grashof numbers clearly showed the uplift of the streamlines from the bottom plate at certain axial locations, suggesting the onset of the vortex flow there. The onset points were also found to advance upstream for a higher Grashof number or a lower Reynolds number. The photos are not shown here due to the limited availability of the space for the article. Tapering the top plate was noted to cause significant delay in the onset of vortex flow at low buoyancy-to-inertia ratio ( $Gr/Re^2$ ). The delay gradually diminished at increasing  $Gr/Re^2$ . At a high  $Gr/Re^2$  no noticeable delay in the onset of vortex flow was detected. Inspecting these side view flow photos for the low Reynolds and high Grashof numbers revealed the presence of irregular recirculating cells and the associated secondary flow was somewhat unstable. This recirculating flow became highly irregular when reaching the downstream portion of the duct. It was also noted that at this high buoyancy-to-inertia ratio

the induced vortex flow was so strong that the forced flow entering the duct was seriously blocked and hence was reversed near the duct inlet resulting in a returning flow there ([23]). More specifically, the returning flow was formed by a part of warm air ascending from the bottom plate slightly upstream of the onset point and penetrating towards the top plate. When the warm air reached the top plate, it split into two streams. One moved upstream and another downstream along the top plate over a certain distance. Meanwhile the upstream moving stream was slowed down by the main forced flow. Finally, it merges with the main flow around the inlet of the heated section. Thus an elongated recirculating cell is formed in the duct entry. It is also noted that after the onset point of thermal instability, most of the test section is dominated by the natural convection for  $Gr/Re^2 \geq 40$ .

To illustrate the effects of the top plate inclination on the detailed vortex flow structures, the instantaneous flow photos from the top and end views were also examined. It was noted from the results for the rectangular duct that at a low buoyancy-to-inertia ratio for  $Re=102$  and  $Gr=2.5 \times 10^4$  a symmetric pair of longitudinal rolls were induced near the side walls beginning at  $z \approx 15$  cm. Slightly downstream at  $z \approx 31$  cm another symmetric pair of longitudinal rolls were generated. This four-roll structure prevailed beyond that. Raising  $Gr$  to  $7.4 \times 10^4$  caused an earlier

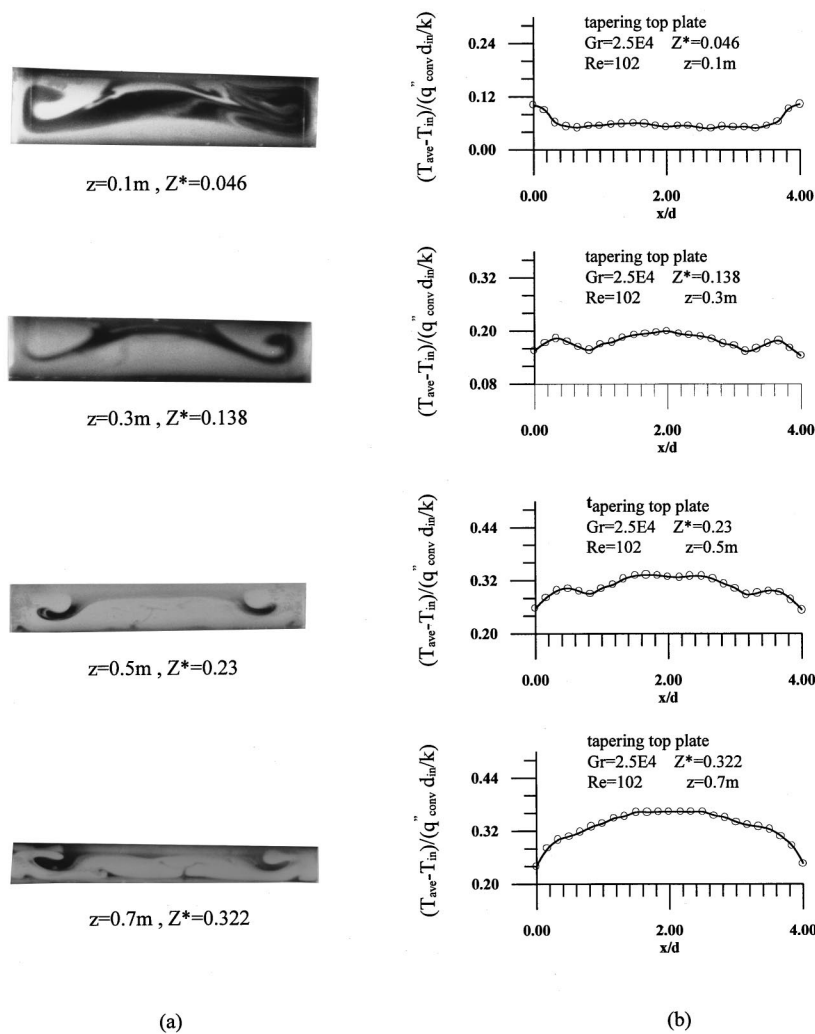
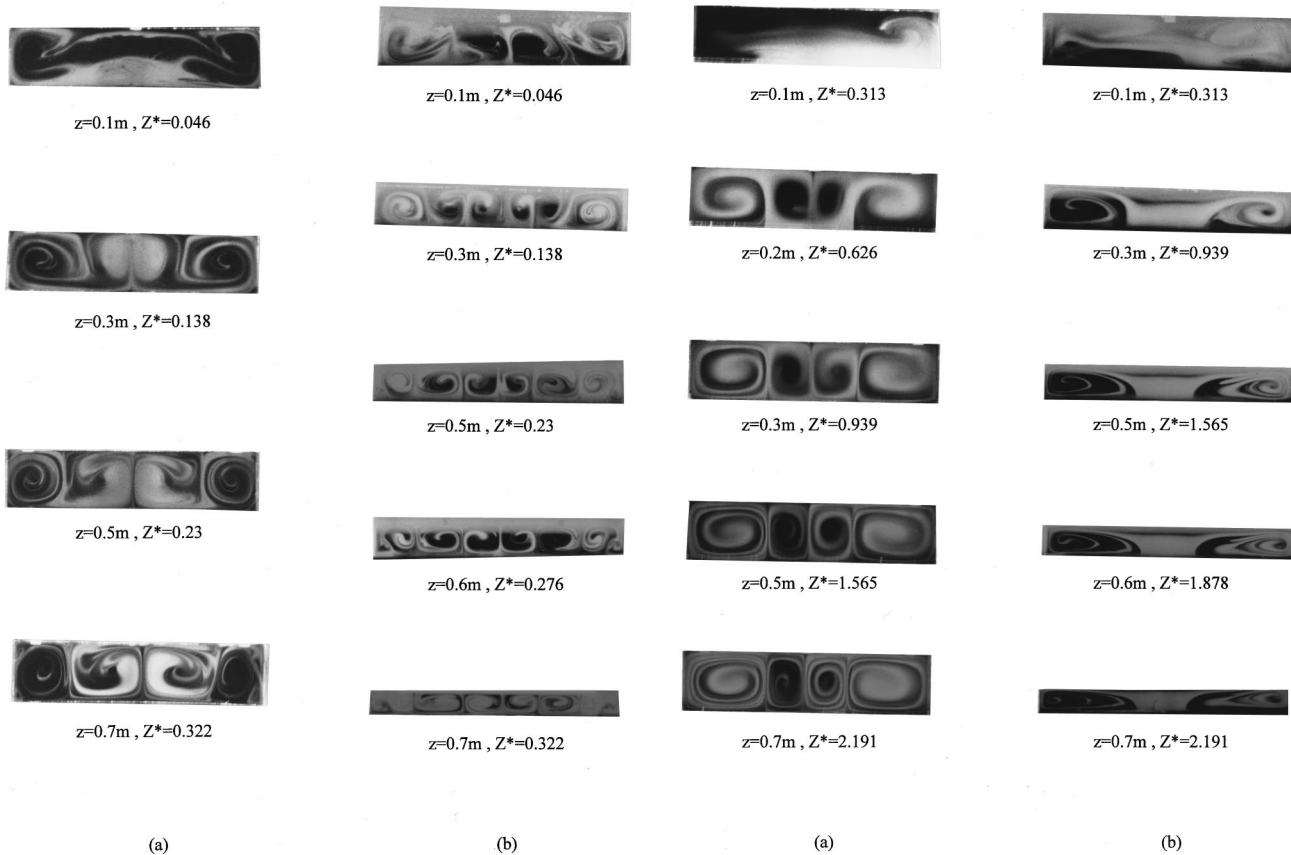


Fig. 5 (a) Instantaneous flow photos and (b) time-averaged spanwise temperature distributions at  $y=1.5$  cm at selected cross sections in tapering duct for  $Re=102$  and  $Gr=2.5 \times 10^4$

onset of the rolls. The vortex flow in the downstream still consisted of four-roll structure. Lowering the Reynolds number from 102 to 88 for  $Gr$  fixed at  $7.4 \times 10^4$  resulted in the generation of a new pair of longitudinal rolls so that there were six longitudinal rolls in the duct. But at this higher  $Gr/Re^2$  the vortex flow is slightly asymmetric with respect to the central vertical plane at  $x=6$  cm. At an even higher  $Gr/Re^2$  the longitudinal rolls were somewhat irregular and were obviously asymmetric. Additional flow photos for the very low Reynolds numbers of  $Re=15$  and  $9$  indicated that the vortex flow still consisted of symmetric longitudinal rolls when  $Gr$  was not too high. Next, snapshots of the flow viewing from the top for the tapering duct at the same  $Re$  and  $Gr$  were inspected. Note that for the low buoyancy-to-inertial ratio case with  $Re=102$  and  $Gr=2.5 \times 10^4$ , a symmetric pair of longitudinal rolls induced in the entry half of the tapering duct were rather weak. At the higher  $Gr$  of  $7.4 \times 10^4$  a pair of stronger longitudinal rolls were induced near the side walls beginning at  $z \approx 8$  cm. At  $z \approx 22$  cm, two plumes of warm air rose near the central vertical plane ( $x=6$  cm) and formed two new pairs of longitudinal rolls. Thus, beyond that we had three pairs of longitudinal rolls in the tapering duct. Lowering the Reynolds number from 102 to 88 for  $Gr$  fixed at  $7.4 \times 10^4$  again caused an earlier appearance of the three pairs of longitudinal rolls. At the even lower

Reynolds number of  $Re=51$ , three symmetric pairs of vortex rolls started to appear at  $z \approx 15$  cm. The results for the low Reynolds number of  $Re=15$  and  $9$  with  $Gr$  fixed at  $1.0 \times 10^4$  for the tapering duct indicated that for  $Re=15$  only one symmetric roll pair was induced near the side walls and no noticeable roll was induced in the center region of the heated section. The rolls near the side walls were suppressed by the accelerating air flow and were weaker than those in the rectangular duct at the same  $Re$  and  $Gr$ . At a lower Reynolds number of  $Re=9$  two pairs of longitudinal rolls began to appear at  $z \approx 16$  cm, one adjacent to the center vertical plane at  $x=6$  cm and another near the side walls. Note that for  $z \geq 30$  cm the two vortex pairs were significantly suppressed by the accelerating main forced flow and their strength got weaker with the downstream distance.

The above observation of the vortex structure changes with the Grashof and Reynolds numbers and with the duct tapering can be further illustrated by the end-view photos for the cross-plane secondary flow at selected cross sections. The corresponding spanwise distributions of the time-averaged air temperature at the mid-height of the duct are also given to quantitatively show the intensity of the vortex rolls. Figure 4 distinctly manifests the evolution of the vortex pattern in the rectangular duct from the uni-



**Fig. 6** Instantaneous and view flow photos at selected cross sections for  $Re=102$  and  $Gr=7.4 \times 10^4$  for (a) rectangular duct and (b) tapering duct

directional flow in the duct entry to the two-roll structure slightly downstream and then to the four-roll structure in the exit half of the duct for  $Re=102$  and  $Gr=2.5 \times 10^4$ . It is also noted from the flow photos and time-averaged temperature distributions that in the upstream ( $z < 0.4$  m) the rolls near the duct sides are stronger than those in the duct core. In the downstream the reverse is the case. The corresponding results for the tapering duct at the same  $Re$  and  $Gr$  are shown in Fig. 5. Note that in the tapering duct one pair of longitudinal rolls clearly exist near the side walls in nearly the entire test section. In the downstream the second pair of longitudinal rolls are rather weak and can be barely seen in the photos for  $z=0.5$  and  $0.7$  m. It is also noted from the time-averaged temperature distributions (Figs. 4(b) and 5(b)) that the strength of the vortex rolls for the tapering duct is much weaker than that in the rectangular duct at the same  $Re$  and  $Gr$ . Further comparison of the results for the higher buoyancies ( $Gr=4.2 \times 10^4$  &  $7.4 \times 10^4$ ) was also made. We noted that the photos for the rectangular duct (Fig. 6(a)) showed a similar vortex flow evolution to that at a lower buoyancy for  $Gr=2.5 \times 10^4$  except the appearance of an additional pair of small vortex rolls near the duct sides in the exit end of the duct. This newly formed vortex pair circulates downwards near the side walls. It should be pointed out that this new vortex pair is small and mainly appears in the duct corners, and hence is not detected by the top view flow photos discussed above in which the secondary flow at the horizontal plane at the mid-height of the duct  $y=1.5$  cm was pictured. Moreover, at these higher buoyancies the rolls in the core region grow significantly as the flow moves downstream. While in the tapering duct an increase of the Grashof number to  $4.2 \times 10^4$  resulted in three pairs of weak longitudinal rolls in the secondary half of the duct. The vortex rolls were obviously weaker than those in the horizontal

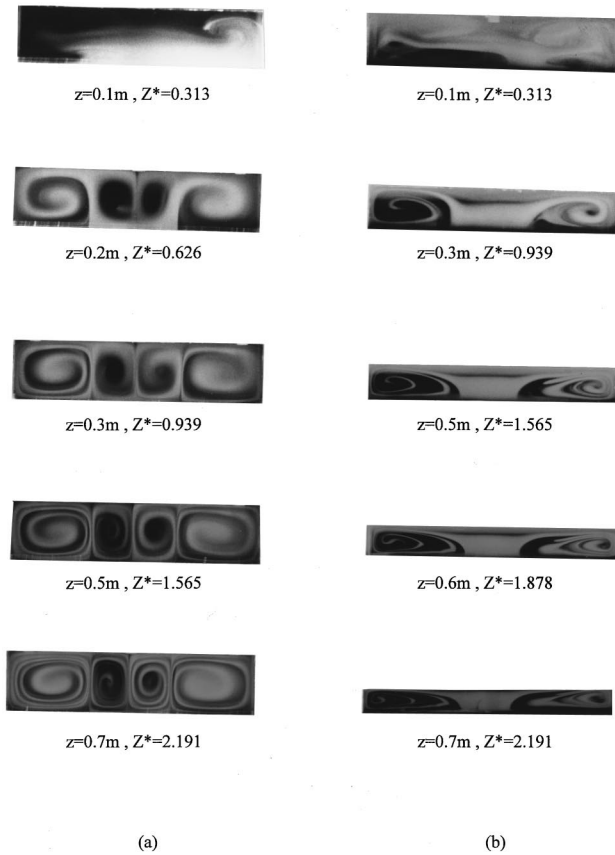


**Fig. 7** Instantaneous end view flow photos at selected cross sections for  $Re=15$  and  $Gr=1.0 \times 10^4$  for (a) rectangular duct and (b) tapering duct

duct. For a higher Grashof number of  $Gr=7.4 \times 10^4$  (Fig. 6(b)) the vortex flow in the tapering duct consists of two weak longitudinal roll pairs in the entry region of the duct core ( $z < 28$  cm), three vortex roll pairs in the middle portion of the duct ( $28 \text{ cm} \leq z \leq 55$  cm), and four pairs in the exit end. Note that due to the flow acceleration in the axial direction associated with the top plate tapering the vortex intensity of the longitudinal rolls does not always increase with the axial distance. For example, the rolls at the cross section  $z=0.7$  m are much weaker than those at the cross section  $z=0.6$  m. These vortex rolls are also weaker than those in the horizontal duct at the same  $Re$  and  $Gr$  (Fig. 6(a)).

The Reynolds number can have a dramatic impact on the vortex flow development, as discussed above. This is further manifested by inspecting the end-view photos for  $Gr=1.0 \times 10^4$  and  $Re=15$  and 9. Note that at these lower Reynolds numbers the vortex rolls in the rectangular duct get stronger with the axial distance but do not merge together (Fig. 7(a)). Moreover, the degree of the vortex flow asymmetry is largest in the duct entry where the vortex flow is relatively weak. Downstream the four vortex rolls are in fact spanwisely symmetric. Note that in the tapering duct only one vortex pair forms at  $Re=15$  (Fig. 7(b)) and the vortex flow is much weaker. At  $Re=9$  there were four rolls induced shortly after the flow entered the duct. But the rolls in the duct core were substantially suppressed by the top plate tapering to nearly disappear in the duct exit. The rolls near the duct sides were also weaker and are in triangular shape. Again the vortex intensity of the flow in the tapering duct is much weaker. For a further reduction of the Reynolds number to 5 the vortex flow quickly evolved to one pair of strong, symmetric longitudinal rolls in the rectangular duct. In the tapering duct the four-pair structure prevailed in the entry half of the duct. Downstream the rolls in the duct core

were significantly suppressed. These downstream rolls were slightly asymmetric. The vortex flow was weakened again by the top plate tapering but in a smaller degree at this low Reynolds number of  $Re=5$ .

To reveal the temporal characteristics of the vortex flow, the time variations of the detected instantaneous air temperature at selected locations for various cases for the rectangular and trapezoid ducts were examined. It was of interest to note that the flow oscillation in the rectangular duct at high buoyancy-to-inertia ratios was completely suppressed by the flow acceleration in the tapering duct. This clearly shows the effective stabilization of the buoyancy driven unstable flow by the top plate tapering.

#### 4 Concluding Remarks

We have performed an experimental study to investigate the effects of the top plate tapering on the stabilization of the buoyancy driven vortex flow in mixed convection of air through the bottom heated horizontal rectangular and tapering ducts by systematic measurement of the time-averaged spanwise temperature distributions and the time histories of the air temperature. Instantaneous flow visualizations were also conducted. The experiments were carried out for the Reynolds number ranging from 5 to 102 and Grashof numbers from  $1.0 \times 10^4$  to  $1.7 \times 10^5$ . The major results can be brightly summarized in the following.

1 In the rectangular duct the onset of thermal instability was found to move upstream for increasing Grashof number and/or decreasing Reynolds number. The results for the tapering duct resemble those for the rectangular duct except that the onset point moves a little downstream as compared with that for the horizontal duct for the same  $Re$  and  $Gr$ .

2 Due to the increase of the aspect ratio from 4 at the duct inlet to 12 at the duct exit, more vortex rolls are induced in the tapering duct than in the rectangular duct in the downstream region.

3 In the tapering duct, the main forced flow accelerates so rapidly in the downstream region that the vortex intensity of the longitudinal rolls are much weaker.

4 The unstable vortex flow at high buoyancy-to-inertia ratio in the rectangular duct can be completely stabilized by tapering the top plate over the range of the parameters covered in the present study.

During the course of this study it has been realized that although the top plate tapering results in the complete stabilization of the vortex flow, the weaker vortices still dominate the secondary flow in the tapering duct. Methods to eliminate these vortices need to be investigated in the future.

#### Acknowledgment

The financial support of this study by the engineering division of National Science Council of Taiwan, R.O.C. through the contract NSC 87-2212-E-009-029 is greatly appreciated.

#### Nomenclature

- $AR$  = aspect ratio,  $b/d$   
 $b, d$  = duct width and duct height  
 $g$  = gravitational acceleration  
 $Gr$  = Grashof number,  $g\beta q''_{conv} d_{in}^4 / k\nu^2$   
 $Gr_z$  = local Grashof number,  $g\beta q''_{conv} z^4 / k\nu^2$   
 $h$  = local convection heat transfer coefficient  
 $k$  = thermal conductivity  
 $L$  = length of the test section  
 $Nu_d$  = Nusselt number,  $hd_{in}/k$   
 $Pr$  = Prandtl number,  $\nu/\alpha$   
 $q''_{conv}$  = local convective heat flux

- $q''_{insul}$  = local conduction heat loss through the insulation  
 $q''_{rad}$  = local radiation heat loss from the surface  
 $q''_{tot}$  = the total heat flux in the plate  
 $Ra$  = Rayleigh number,  $Gr \cdot Pr$   
 $Re$  = Reynolds number,  $\bar{w}_{in} d_{in} / \nu$   
 $Re_z$  = local Reynolds number,  $\bar{w} z / \nu$   
 $T$  = temperature  
 $w$  = velocity component in axial direction  
 $x, y, z$  = Cartesian coordinates  
 $X, Y, Z$  = dimensionless Cartesian coordinate,  $x/d_{in}$ ,  $y/d_{in}$ , and  $z/d_{in}$   
 $Z^*$  = modified Z-coordinate,  $z/d_{in} \cdot Re \cdot Pr$   
 $\beta$  = thermal expansion coefficient  
 $\nu$  = kinematic viscosity

#### Subscripts

- $b$  = of buck quantities  
 $in$  = values at the inlet of the test section  
 $w$  = of heated wall quantities

#### Superscripts

- = average value

#### References

- [1] Mori, Y., and Uchida, Y., 1996, "Forced Convective Heat Transfer Between Horizontal Flat Plates," *Int. J. Heat Mass Transf.*, **9**, pp. 803–817.
- [2] Akiyama, M., Hwang, G. J., and Cheng, K. C., 1971, "Experiments on the Onset of Longitudinal Vortices in Laminar Forced Convection Between Horizontal Plates," *ASME J. Heat Transfer*, **93**, pp. 335–341.
- [3] Ostrach, S., and Kamotani, Y., 1975, "Heat Transfer Augmentation in Laminar Fully Developed Channel Flow by Means of Heating From Below," *ASME J. Heat Transfer*, **97**, pp. 220–225.
- [4] Kamotani, Y., and Ostrach, S., 1976, "Effect of Thermal Instability on Thermally Developing Laminar Channel Flow," *ASME J. Heat Transfer*, **98**, pp. 62–66.
- [5] Hwang, G. J., and Liu, C. L., 1976, "An Experimental Study of Convective Instability in the Thermal Entrance Region of a Horizontal Parallel-Plate Channel Heated From Below," *Can. J. Chem. Eng.*, **54**, pp. 521–525.
- [6] Incropera, F. P., Knox, A. L., and Maughan, J. R., 1987, "Mixed-Convection Flow and Heat Transfer in the Entry Region of a Horizontal Rectangular Duct," *ASME J. Heat Transfer*, **109**, pp. 434–439.
- [7] Maughan, J. R., and Incropera, F. P., 1990, "Regions of Heat Transfer Enhancement for Laminar Mixed Convection in a Parallel Plate Channel," *Int. J. Heat Mass Transf.*, **33**, pp. 555–570.
- [8] Mohareri, S. S., Armaly, B. F., and Chen, T. S., 1988, "Measurements in the Transition Vortex Flow Regime of Mixed Convection Above a Horizontal Heated Plate," *ASME J. Heat Transfer*, **110**, pp. 358–365.
- [9] Chiu, K. C., and Rosenberger, F., 1987, "Mixed Convection Between Horizontal Plate—I. Entrance Effects," *Int. J. Heat Mass Transf.*, **30**, pp. 1645–1654.
- [10] Chiu, K. C., Ouazzani, J., and Rosenberger, F., 1987, "Mixed Convection Between Horizontal Plates—II. Fully Developed Flow," *Int. J. Heat Mass Transf.*, **30**, pp. 1655–1662.
- [11] Nyce, T. A., Ouazzani, J., Durand-Daubin, A., and Rosenberger, F., 1992, "Mixed Convection in a Horizontal Rectangular Channel—Experimental and Numerical Velocity Distributions," *Int. J. Heat Mass Transf.*, **35**, pp. 1481–1494.
- [12] Ouazzani, M. T., Caltagirone, J. P., Meyer, G., and Mojtabi, A., 1989, "Etude Numerique et Experimental de la Convection Mixte Entre Deux Plans Horizontaux," *Int. J. Heat Mass Transf.*, **32**, pp. 261–269.
- [13] Ouazzani, M. T., Platten, J. K., and Mojtabi, A., 1990, "Etude Experimental de la Convection Mixte Entre Deux Plans Horizontaux a Temperatures Differents—II," *Int. J. Heat Mass Transf.*, **33**, pp. 1417–1427.
- [14] Yu, C. H., Chang, M. Y., and Lin, T. F., 1996, "Structures of Moving Transverse and Mixed Rolls in Mixed Convection in a Horizontal Plane Channel," *Int. J. Heat Mass Transf.*, **40**, pp. 333–346.
- [15] Cheng, K. C., and Shi, L., 1994, "Visualization of Convective Instability Phenomena in the Entrance Region of a Horizontal Rectangular Channel Heated From Below and/or Cooled From Above," *Exp. Heat Transfer*, **7**, pp. 235–248.
- [16] Koizumi, H., and Hosokawa, I., 1993, "Unsteady Behavior and Mass Transfer Performance of the Combined Convective Flow in a Horizontal Rectangular Duct Heated From Below," *Int. J. Heat Mass Transf.*, **36**, pp. 3937–3947.
- [17] Huang, C. C., and Lin, T. F., 1994, "Buoyancy Induced Flow Transition in Mixed Convective Flow of Air Through a Bottom Heated Horizontal Rectangular Duct," *Int. J. Heat Mass Transf.*, **37**, pp. 1235–1255.
- [18] Huang, C. C., and Lin, T. F., 1995, "Vortex Flow and Thermal Characteristics in Mixed Convection of Air in a Horizontal Rectangular Duct: Effects of

Reynolds and Grashof Numbers," *Int. J. Heat Mass Transf.*, **38**, pp. 1661–1674.

- [19] Lin, W. L., and Lin, T. F., 1996, "Experimental Study of Unstable Mixed Convection of Air in a Bottom Heated Horizontal Rectangular Duct," *Int. J. Heat Mass Transf.*, **39**, pp. 1649–1663.
- [20] Lin, W. L., Ker, Y. T., and Lin, T. F., 1996, "Experimental Observation and Conjugate Heat Transfer Analysis of Vortex Flow Development in Mixed Convection of Air in a Horizontal Rectangular Duct," *Int. J. Heat Mass Transf.*, **39**, pp. 3667–3683.
- [21] Kline, S. J., and McClintock, F. A., 1953, "Describing Uncertainties in Single-Sample Experiments," *Mech. Eng.*, **75**, pp. 3–8.
- [22] Tseng, W. S., 1996, "Stabilization of Mixed Convective Air Flow in a Bottom Heated Rectangular Duct by Tapering its Top Plate," M.S. thesis, National Chiao Tung University, Hsinchu, Taiwan, R.O.C.
- [23] Visser, E. P., Kleijn, C. R., Govers, C. A. M., and Hoogendoorn, C. J., 1989, "Return Flows in Horizontal MOCVD Reactors Studied With the Use of TiO<sub>2</sub> Particle Injection and Numerical Calculations," *J. Cryst. Growth*, **94**, pp. 929–946.